A Novel Dual Time-Point Unified Amyloid MRI/PET Data Analysis Technique

Vipul Vekariya
Department of CSE, PIET,
Parul University,
vipul.vekariya18435@paruluniveristy.ac.in

Alka Kumari
Department of Computer Science,
ARKA JAIN University,
alka.k@arkajainuniversity.ac.in

2023 International Conference on Artificial Intelligence and Smart Communication (AISC) | 979-8-3503-2230-9/23/$31.00 ©2023 IEEE | DOI: 10.1109/AISC56616.2023.10084979

***Abstract*- There is disagreement regarding the best method for performing semi-quantified of amyloid in the preliminary assessment of sufferers with suspicious Alzheimer's & dementia illness in order to: (1) enable picture subjective explanation; (2) account for the propulsive actions of the detector, especially when it comes to at partly adjusting for blood circulation reliance; (3) evaluate the amyloid burden utilizing precise segmentation of subcortical & cortical region.**

Methodologies Comprehensive testing of a technique that included all of these features was performed on eighty-six patients who had amyloid (18F-florbetaben) MRI/PET in a medical context . After injecting the detector, early photos were taken within 0 & 10 minutes later, while subsequent pictures were taken around 90 & 110 minutes later. Utilizing the geometrical transferring matrix technique, PVEC of the PET information was done. 2 novel Bdual time-point indices as well as parameterized pictures as well as certain local expected outputs were established.

According to the is cortical phase of the topographical arrangement of the amyloid plaques, the main sensor, neurological, & retinal regions of patients who were categorised subjectively as amyloid +Ve displayed a scant tracer pickup. The technique identified trace levels of tracer take - up in the basal parts of the temporal & frontal lobes in sick people who were visibly determined to be amyloid—Ve. These areas are thought to be locations of beginning amyloid plaque accumulation & likely symbolised beginning concentration , which is usual of aging process. In individuals who tested negative for amyloid, the results showed a significant association within age as well as the indices of the novel dual time-point amyloid picturing technique.

The approach will standardise information on amyloid concentration, making it a useful instrument for both ordinary clinical practise as well as the research context. In younger people, when therapy would hypothetically be more successful, it might also be utilised to detect beginning amyloid plaque formation.

Keywords-MRI/PET, Quantification, tracers for amyloid, dual time points, Dementia, Alzheimer's disease (AD)

I. INTRODUCTION

In order to identify or rule out cerebral amyloid deposition as the underlying disease in individuals with cognitive loss, amyloid PET scanning is rapidly being employed in normal medical care. Furthermore, recent investigations [1] have shown that even among some healthy individuals in between ages of fifty through eighty-nine absent signs of mental deterioration, a certain degree of cerebral amyloid build-up might be regarded an average follow - up of neurodegenerative disorders. When individuals are eighty-nine years old, 80.00% of them had cerebral amyloid deposition, abnormal development, or even both, at comparable levels with those found in the brains of people with AD. Up to 28.00% of normal subjects have amyloid deposit in the brains when they are youthful, however atrophy is only occasionally (approximately 5.00%) linked to amyloid deposition. The importance of amyloid Neuroimaging currently rests on its -Ve forecast value in the context of these results. Amyloid PET research findings are helpful to rule out AD under strictly focused circumstances marked by diagnosing ambiguity, like in patients with frontal temporal dementia & early - onset atypical AD, or to supply physiological data needed for clinical tests of illness purpose of treatment amyloid, as per abilities guidance [2, 3].

On the foundation of qualitative subjective evaluations of PET pictures, recent crucial PET investigations with histological verification [4-6] came to their main results. Producers' guidelines that have been authorized by the European Medicines Authority advice [7-9] that a quality visual assessment of neurofibrillary be carried out by nuclear medicine experts with the assistance of CT / MRI images.

Numerous statistically valid techniques, centred on PET by itself [11–15] or on combined techniques [16, 17], have reduced the ambiguity in some cases. These techniques merely use the cerebral grey matter or the entire cerebrum as the benchmark region because utilisation trends in that area of the brain are comparable in AD sufferers and in control subjects [10]. It's fascinating to observe that while at the same moment, a few investigators [18] have noted that statistical approach for data capture as well as kinetic assessment are in every case required in observational research because quasi methodologies lack accuracy and thus are impacted by modifications in the brain's blood flow related to illness advancement. Considering the requirement for amyloid burden measurement, only a small number of investigations have looked at the standard in terms of amyloid imaging techniques utilizing complete kinetics assessment [19–21]. This research used 18F-florbetaben.

There is currently no definitive agreement on the best way to do amyloid quasi, as well as no straightforward approach for the quasi of cerebral amyloid burden that simultaneously: (1) considers the tracer's kinematic activity, especially in relation to lowering the plasma circulation element in estimations of -amyloid burden,(2) provides a description of the amyloid useful indication on precise dissection of subcortical & cortical regions, (3) incorporates short channel impact adjustment of PET information, (4) incorporates MRI performance measures , (5) could be implemented to PET & MRI captured images concurrently, & (6) could be done automatically.

Therefore, we describe a technique that satisfies each of these criteria & evaluate it using data from an 18F-florbetaben MRI/PET scan. The practises here as well yields two novel semi-quantification indices, which are described &

evaluated versus fixed threshold value ratios adjusted for PVE & MRI measurements.

II. Materials And Methods

A. Study participants

86 individuals' worth of information was used to retroactively evaluate the data mining technique. Among these participants, 53 were primarily determined as amyloid-negative,& 33 (average age 71 Among these participants, 53 were primarily determined as amyloid-ve,& 33 (average age 71+- 10 years) A identified independent reading was used to settle discrepancies in ratings (8 individuals, 9.30%). There have been 22 cases of moderate cognitive decline, 1 dementia of Cell bodies, 4 cases of behaviour variations frontal lobes deterioration, 14 cases of suspicious AD, 8 cases of likely AD, 2 cases of anomalous AD, & 2 cases of blended dementia in the amyloid-negative sick people. Before having their brains imaged using brain MR/PET and analysing the resulting experimental evidence, all individuals gave their explicit, written consent.

B. Possession & restoration of images

Fig. 1 depicts every stage of the picture data collecting & treatment process. The participants underwent an intravenous infusion of approximately 0300 MBq 018F-florbetaben directly in an incorporated 3-T MRI/PET system in relate with the amyloid picturing procedure rules. Brain pictures were taken between 0 and 10 minutes following the infusion of the tracker , as in earlier research [22, 23]. After then, the participants were free to exit the scanning. Around 90 & 110 minutes following the infusion, later photos were taken. The obtained PET information were rebuilt utilising constructed three - dimensional objects order sets expectations maximisation technique with 8 iteration, 21 subset, & a 3-mm Gaussian filter together into 256*256 matrix . Appropriate attenuation, degradation, scattering, & dead time adjustments were made. For contrast enhancement, a 2-point MRI Dixon VIBE series with the following parameters was utilized: TR 03.60 ms, TE 01.230 ms, layer thick 03.120 mm, matrices 256*256, FOV 500*300 mm, segmentation attenuation constant maps. Simultaneous to the PET acquisitions, anatomic information was also acquired using a 3-dimensional T1 magnetization-prepared fast acquiring gradients echo series.

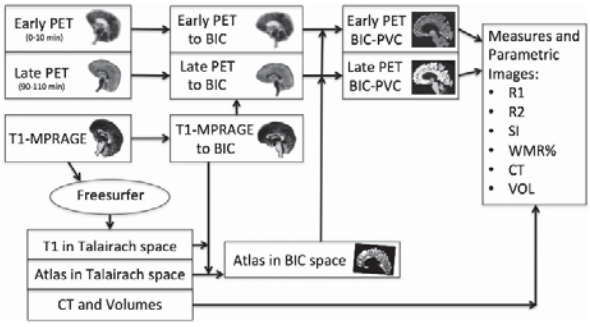

Fig. 1. is a schematic diagram illustrating the key actions in the suggested semi-quantitative method [57].

C. Construction of a sufferer specific atlas

Free Surfer (v. 5.3) program was used to handle the T1-weighted (T1w) MR pictures for fragmentation & cortical parcellation. In a nutshell, the procedure involved extracting non-brain cells [24], automating Talairach space transform, segmenting subcortical white subject & deep gray matter volume frameworks [25, 26], intensifying the grey & white matter border [27], automating configuration adjustment [28, 29], and deforming the area. The cerebrum was subsequently divided into sections depending on the sulcal& gyral features [30]. Regional cortical thickening was calculated using data from the whole 3-dimensional MRI region [31].

With each cortical region, the following findings were attained: the customer centred atlas utilized to name the participant's brain regions in line with the Desikan-Killiany cortex naming method [30], the source T1w pictures converted further into Talairach format, as well as the text documents containing the brain thickness & volume.

D. Data processing for images

The source T1w MRI database were rigidly transformed to the adjusted MNI152 1-mm reference area [32] and realigned along the bi-commissural line (BIC) (ANT). The same processing variables were used on all PET information recorded between 90 and 110 minutes following infusion. The BIC spatially T1w MR Pictures were then tightly aligned to the 0–10 minute PET information. Interpolation registrations was used to normalise the Talairach spatially T1w MR Pictures (created with Free Surfer) to the BIC spatially T1w MR Pictures. The Desikan-Killiany atlas information was then subjected to a similar affinity utilizing the nearest-neighbour interpolated method in order to shield it against segmentation misunderstanding. 3 kinds of aligned pictures (T1w MRI, Desikan-Killiany& PET atlas) were acquired in the BIC region using this method. In spite of deformations brought about by transformation to standards dimensions, this permitted verification of the accurate attribution of the atlas sections to the anatomical regions. Additionally, this method made it possible to utilize the atlas VOIs in PVEC of PET information that was not distorted.

E. Algorithmic outputs

The following regional outcome variables, depending on the VOI, were extracted [33-36] using an automation specialised internal computer program:

1) PVEC1: Main work density (kBq/cm3) of a PVE-rectified PET information recorded shortly just after infusion of the amyloid marker.

2) PVEC2: Main activity volume (kBq/cm3) of the PVE-rectified PET information recorded immediately after the infusion of the amyloid marker.

3) PVEC1focus VOI/PVEC1Cerebellar cortical equals R1Tfocus VOI. It needs to be highlighted that while being strongly affected by blood circulation, the brain pictures acquired shortly after marker injection (R1) only provide for a rough estimation of blood circulation rather than a direct measure. Furthermore, this method may serve as a remedy in the lack of absolute quantification as well as the ensuing K1 function approximation.

4) PVEC2 focus VOI/PVEC2 Cerebellar cortex equals R2 focus VOI. According to published studies [33, 34], the R2 indicator measures an object that is usually known as BSUVr and which was also rectified for PVE in this study. As a result, the SUV represented by the R2 score is state-of-the-art.As a result, the SUV represented by the R2 score is state-of-the-art.

5) SI (gradient index) = (R2Target VOI R1Target VOI)/(T2Target VOI T1Target VOI), wherein T2 & T1 are the beginning timings of the late & early collections following the management of the amyloid marker, respectively. By showing a gradient, this variable incorporates the information from the two amyloid PET time windows (Fig. 2). A positive sign denotes a difference between the local blood circulation surrogate (R1) & the local amyloid burden, & vice versa.

A positive sign denotes a difference between the local blood circulation surrogate (R1) & the local amyloid burden, & vice versa.

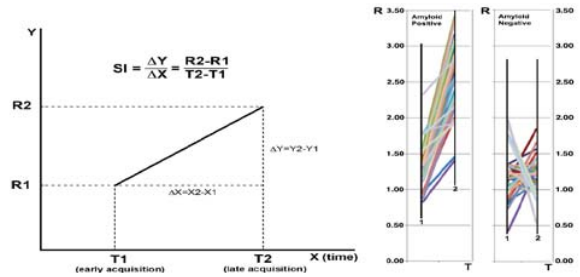

Fig. 2. Gradient index diagrammatic representation (SI, left). The opening hours for late & early PET scans following [57] amyloid marker infusion are T1 & T2, accordingly.

6) Fig. 3 provides a graphic representation of such a index. Since new research [37] has demonstrated that the white matter is a good reference area for longitudinally evaluations of cerebral amyloid burden, it was chosen as the variable's reference area. Since new research [37] has demonstrated that the white matters are a good reference area for longitudinally evaluations of cerebral amyloid burden, it was chosen as the variable's reference region.

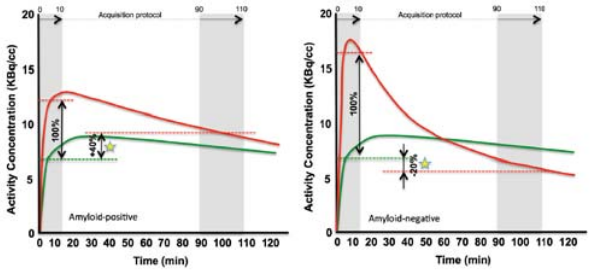

Fig. 3. The WMR % score is depicted [57] schematically.

The constant red line indicates the activity concentration with duration in a cortical region of a subject who was physically diagnosed as amyloid +ve (left) & a subject who was physically classed as amyloid -ve (right).

7) Cortical thickness in millimetre.

8) Cortical volume in millimetre cube.

The program also delivered the appropriate descriptive pictures in addition to these geographical data.

F. *Statistical assessment*

SAS 9.4 for Window was used to conduct the data study. To determine if the data was evenly distributed, the Shapiro-Wilk examination was carried out. Depending on the distribution's normalcy, the Patient's sample t - test or the Mann-Whitney testing was used to analyse individuals with & without amyloid. Cohen's d was used to determine sample size. In individuals who tested -Ve for amyloid, Spearman's co-relation factor was used to assess co-relations among local amyloid PET values, aged, as well as MRI variables. Amyloid PET variables' capacity to distinguish between the 2 treatments populations was assessed using receiver operating characteristic (ROC) waves analysis, with the findings represented as regions underneath the curve & 95.00% confidence intervals (CI). The 5.00% statistical significance level was chosen.

III. Results

Supplemental Table 1 displays results for all program response variables for all VOIs examined in amyloid-+Ve and amyloid -Vesufferers & Table 1 groups these findings by anatomical locations.

R1 showed a negligible Cohen's d impact factor (00.440) among individuals identified physically as amyloid- -Ve& amyloid +Ve in the total brain imaging. The prefrontal & insular lobe, as well as the core regions, has greater Cohen's d values (00.20 to 00.50), according to a lacunar study of R1. There was tiny Cohen's d response size for the frontal lobes, but there was no difference among amyloid—Ve and amyloid +ve individuals overall in the brains according to CT . R2, SI, & WMR percentage were, therefore, considerably greater in the brains overall in amyloid-+ve sufferers in comparison to amyloid -ve patient populations. R2, SI, & WMR% had significant Cohen's d treatment effects in the nervous system (03.870, 03.680, & 02.020, correspondingly). With the exception of WMR percentage for the right temporal lobe, each indicator (R2, SI, & WMR %) displayed high Cohen's d acting for each lobe . Amyloid +ve individuals had reduced overall levels of VOL in the brains (Fig. 4), with a moderate Cohen's d impact magnitude on the left (00.540) & a moderate effect value on the right.

Figures 5 & 6 display results for all program outcome parameters for every VOIs examined in individuals with and without amyloid deposits. The prefrontal, temporal, insular, & occipital lobe showed the greatest standard deviation among amyloid +ve& amyloid -ve individuals for R2 (Fig. 5). The same applied to SI & WMR% (Fig. 6).

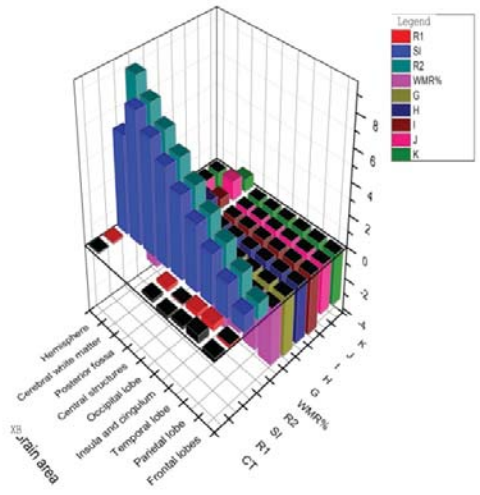

Fig. 4. statistics for each key brain structure's outcome parameters from all programs.

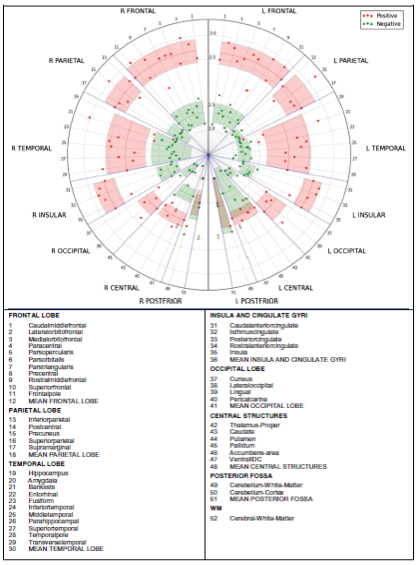

Fig. 5. Median R2 indices value for each region of the brain [57]

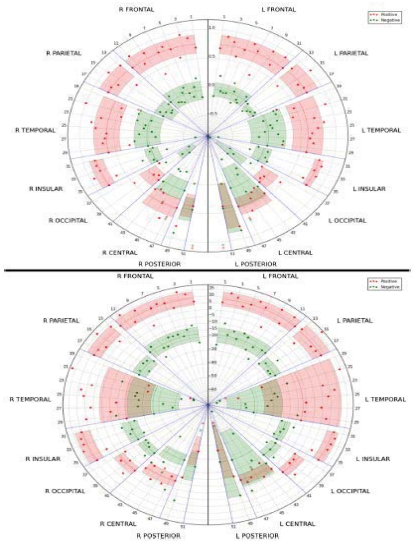

Fig. 6. depicts the median SI & WMR % index readings for each region of the brain [57].

According to the EMA's [7-9] recommendations, ROC wave shape were generated by visual examination of the amyloid information recorded close to the end after detector administration as the base classification. In the whole nervous system, R2, SI, & WMR % used to have elevated discriminatory practices precision [00.9870, 00.97300, & 0.9360, correspondingly], while Computed tomography, R1, & VOL seemed to have reduced discrimination precision (00.50800, 0.6290 & 00.6400, correspondingly). The ROC findings indicate minute inter-lobar variations in the study variables (Supplementary Fig. 1).

The VOI-centred results and the photographs by the parametric programme (Fig. 7) agreed well. Whereas the R2, SI, & the +ve amplitude WMR % photos demonstrated the typical photographing differences among amyloid -ve& amyloid +ve individuals, the average R1 pictures did not substantially vary among amyloid-+ve& amyloid -ve patient populations. Intriguingly, the global brain SI pictures of the amyloid -ve population showed measurable trace accumulation in the mesio-temporal, hippocampus, & entorhinal frontal cortex (Fig. 6).

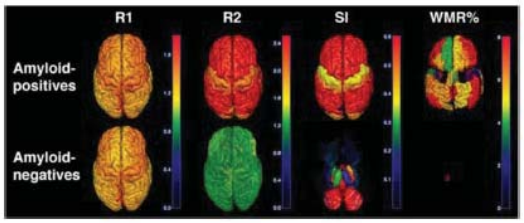

Fig. 7. 3D parametric surface projecting pictures for R2, R1, R2 , SI, & the +ve value of the WMR % in amyloid +ve individuals & amyloid -ve clients, as seen from below. [57]Scaling the corresponding index photos to the exact interval.

Just at lobar & global sight, the response variables (R2, R1, SI & WMR %) and aging revealed significant connections approaching relevance for R2 in forty-five regions, for SI in sixty-eight areas, & for WMR % in seventy-two areas in amyloid -ve individuals (Table 2, Figs. 2 & 3). In amyloid -ve individuals (Table 2), the Spearman's rank correlation values for SI was greater than those for R2 & WMR %. R2, WMR %, & SI, inside the left parietal lobes, left temporal lobes, & right temporal lobe, correspondingly, didn't statistically relate with patient's age. R2 did not substantially relate with VOL, VOI, or CT in amyloid -ve individuals, while SI & WMR % did in 3 lobar locations (Table 2). S1, R2, & WMR % have only been linked to age at the sub-lobar stage in the right entorhinal region, right Para hippocampal region, & left rostral mid frontal region in amyloid +ve patient populations (p = 00.0020, p =0 0.0050, and p = 00.0150, correspondingly). SI was only linked to age in the right parahip-pocampal region & only WMR % was co-related with aging in the left. Neuro-degenerative indices & amyloid burden indices were also strongly inversely associated in amyloid +ve individuals, with the exception of the internal lobe (Figs. 4 & 5).

IV. Discussion

The demand for technologies that can evaluate multi-modal picturing data is on the rise because to the growing attention in adding multi-modality picturing-based bio-marker in diagnosis methods for AD [38]. The innovative method examined in this study & put forward here, which combines structure MRI & dual period point amyloid PET scanning information, shows that this information can be combined to yield useful diagnostics.

Till far, 4 different kinds of methods—manual, PET, MR-centred, & absolute quantification—have been employed to quantify or semi-quantitatively assess amyloid burden. Manually defining zones of concern is a lot of effort & has poor repeatability. PET techniques use later acquisition & are built on tinplating [13, 17, 39, 40], adaptable patterns with orthogonal surface projections [41, 42] or even without [14, 42], multi-atlases & 3-D [43], & median atlases [44]. When comparing to MR centred SUVR, median atlas, adaptable atlas, & multi-atlas techniques are linked to inaccuracies in SUVr measurement [11] of 05.60%,0 3.060%, and 02.740%, correspondingly. A SUVR alone [15] method (ELBA) relying on brightness distributions instead of real VOI values or PiB prone areas of

TABLE II. THE CORRELATION AMONG AGING, MRI VARIABLES, & LOCAL AMYLOID PET VARIABLES IN THE LEFT PART IN INDIVIDUALS WHO WERE QUALITATIVELY IDENTIFIED AS AMYLOID -VE BY BLIND USERS ANALYSING THE BRAIN IMAGING

Brain area	Index	Patient age		CT		VOL	
		p value	Correlation coefficient (r)	p value	Correlation coefficient (r)	p value	Correlation coefficient (r)
Temporal	SI	0.0002**	0.49a		n.s.	0.0348*	−0.29a
	WMR%	0.0051*	0.38		n.s.		n.s.
	R2	0.0004**	0.47		n.s.		n.s.
	R1		n.s.		n.s.		n.s.
Frontal	SI	0.0005**	0.46a		n.s.	0.0523	−0.27
	WMR%	0.0254*	0.31		n.s.		n.s.
	R2	0.0496*	0.27		n.s.		n.s.
	R1		n.s.		n.s.		n.s.
Parietal	SI	0.0007**	0.45a		n.s.		n.s.
	WMR%	0.0105*	0.35		n.s.	0.0236*	−0.31a
	R2		n.s.		n.s.		n.s.
	R1		n.s.		n.s.		n.s.
Occipital	SI	0.0020*	0.42a	0.0261*	n.s.		n.s.
	WMR%	0.0059*	0.37		−0.31	0.0186*	−0.32a
	R2	0.0155*	0.33		n.s.		n.s.
	R1		n.s.		n.s.		
Insular	SI	0.00001**	0.57a		n.s.	0.0514	−0.27
	WMR%		n.s.		n.s.		n.s.
	R2	0.03724*	0.29		n.s.		n.s.
	R1	0.0002**	−0.49		n.s.		n.s.
Total (left	SI	0.0013*	0.43a		n.s.		n.s.
hemisphere	WMR%	0.0065*	0.37		n.s.		n.s.
	R2	0.0255*	0.31		n.s.		n.s.
	R1		n.s.		n.s.		n.s.

focus [45] created by removing -ve from +ve patterns are 2 additional, more current methods for assessing amyloid deposit. FreeSurfer program [40, 46, 47], the FAST & FIRST FSL packages [14], or PMOD are some of the normalisation tools used by MR centred approaches. The utilization of automated reference extract was also made for standard in terms utilising comprehensive kinetics modeling, either with simultaneous arterial sample [19] or even without it [48]. Some [50] also employed parameterized scanning & kinetics analytics to reduce bias brought on by the choice of anatomical area.

The suggested technique, however, utilises a streamlined auto vibrational assessment that also accounts for a blood circulation substitute ,& as a result, contains incomplete adjustment for blood circulation reliance. To our understanding, neither of the procedure listed employs a dual timeframe.

Even though numerous arterial sample size & metabolite adjustment along with vibrant absolute amyloid capacity quantitative would be the optimal strategy for verifying our technique, this isn't a realistically accessible remedy, particularly in demented inhabitants& in a healthcare setting. Additionally, we added MR-centred PVEC with dissection in our approach as a component of the dual processing step in light of the fact as PVEC has been demonstrated as a technique that enhances the analytical ability to detect longitudinally alterations or across variations [51]. Examining local variations in amyloid loading in numerous segmental as well as at least partly blood flow-dependent neurons is facilitated by the combination of the dual period PET & PVEC.

Using PVEC, the new method rapidly generates a variety of useful indices by analysing multiple subcortical & cortical regions. It could result in a more precise quasi assessment that considers the dynamic activity of the marker rather than depending on the Bstatic indices, as was shown with the recently suggested SI & WMR % indices. This merits additional examination in long-term investigations and may at least partly compensate for the amyloid bourdon's reliance on blood circulation. The cerebral width as well as the size of the segmentation sections is also acquired from the structural Magnetic resonance data analysis in additional to the double time-point amyloid PET information.

One benefit of the technology is that it goes beyond the conventional visual interpretation of amyloid PET scans, which yields binary Local result variables and assessments of the entire brain can both be achieved. This result is in line with the is cortical phase of amyloid plaque topography dispersion, as classed by Braak as well as Braak and also other scholars [52-54], where the SI, the WMR %, &, to a smaller extent, the R2 metrics had shown relatively limited sampling take - up in only certain regions. These findings were found in patient populations who were visibly categorised as amyloid -ve . These results appear to show that individuals who are categorised subjectively as amyloid -ve really have some deposition of amyloid plaque. Intriguingly, this was the situation in 008 out of 053 individuals (15.00%) who had been assigned by neurology primarily for memory disorders and who were medically characterised as having likely AD or in which amyloid -ve could be verified. According to our observations, a new analysis [55] has revealed that patients who test -ve for amyloid have a variety of clinical manifestations.

Whenever the local amyloid PET data have been evaluated in relationship to age in the amyloid +ve participants, no aged related connection was discovered in the majority of regions of the brain, which would have been anticipated if the plaque concentration mentioned above could be regarded an amyloid sack pretty standard of normal ageing and identified by the new technique. This result supports the theory that the accumulation of amyloid in the MCI phase already has peaked [1, 56]. A contrasting pattern was seen in the amyloid -ve participants, where there was a substantial inverse relationship among aging as well as marker pickup in numerous of the locations studied. Further evidence that thermal indicators are preferable to static index values for tracking regular accumulation with age originates from the fact that in sick people who were classed as amyloid -ve, thermal indicators co-related better with years. If more studies support these findings, the technique will be beneficial for both research fields as well as ordinary medical interpretation of data considering that visually binary readings are insufficient for tracking therapy obey.

The suggested technique simply generates a customer assessment of a proxy for perfusion (R1), cerebral thickness (CT), & size in conjunction to kinetic indicators and R2. Just a small quantity of regions (Table 1), particularly the forehead, insular, & central regions, showed CT, R1 & VOL differences among amyloid +ve& amyloid -ve individuals. Because some clients with amyloid bunch need not exhibit neuro-degeneration, as well as some clients with neuro-degeneration need not showed considerable amyloid burden , these less obvious distinctions especially in comparison to those noted with other indicators (SI, R2, WMI %) would primarily be predicted at the collective level. Additionally, in the amyloid +ve sample, decreases in lobar VOL &CT were substantially & indirectly linked with R2, SI, & WMR % (Figs. 4 & 5). The observation that all these connections are stronger for double time-point indices than for R2 than that for R2 supports the idea that the original suggestion is worthwhile. The insula, which is notoriously difficult to separate due to the nearby grey tissues, is the sole essential lobes when it comes to segment (Figs. 4 & 5).

The R2 metric was successful in differentiating between amyloid +ve and negative, as evidenced by a ROC curve area of 00.9870. However, in the ROC evolution SI & WMR % at the entire brain levels seemed to be somewhat poorer than R2. Because SI & WMR % are kinematic indices, it follows that they also take into account data from R1, which is not assessed by either the critical review or the R2 indicator. It appears that R2 is marginally more effective at differentiating between amyloid +ve and negative as judged subjectively at the moment (T2) whenever the R2 score is produced & that R2 isn't always a superior way to categorise the disease in real numbers.

V. Conclusions

We describe a brand-new semi-quantitative approach that integrates local a double time-point amyloidosis PET & MRI information processing to quantify -amyloid accumulation. The amyloid data is at least partly adjusted for blood circulation dependent in addition to shrinkage & spillover inaccuracies. Furthermore, the technology described here technically makes both pathophysiology pictures & topographical indicator photos available, providing a multi-biomarker perspective of the intellectually damaged brain.

It will show to be a useful method for detecting early phase illness in younger patients in whom medication is likely to be easily beneficial if the validity of the simpler double time-point evaluation in detecting early diagnosis phases is verified by continuous & follow-up investigations.

References

[1] Jack CR Jr, Wiste HJ, Weigand SD, Rocca WA, Knopman DS, Mielke MM, et al. Age-specific population frequencies of cerebral β-amyloidosis and neurodegeneration among people with normal cognitive function aged 50-89 years: a cross-sectional study. Lancet Neurol. 2014;13(10):997–1005.

[2] Guerra UP, Nobili FM, Padovani A, Perani D, Pupi A, Sorbi S, et al. Recommendations from the Italian interdisciplinary working group (AIMN, AIP, SINDEM) for the utilization of amyloid imaging in clinical practice. Neurol Sci. 2015;36(6):1075–81.

[3] Centers for Medicare and Medicaid Services. Decision Memo for Beta Amyloid Positron Emission Tomography in Dementia and Neurodegenerative Disease (CAG-00431N). Updated 27 September 2013. https://www.cms.gov/medicare-coverage-database/details/nca-decision-memo.aspx?NCAId=265. Accessed 11 Jun 2017.

[4] Sabri O, Sabbagh MN, Seibyl J, Barthel H, Akatsu H, Ouchi Y, et al. Florbetaben PET imaging to detect amyloid beta plaques in Alzheimer's disease: phase 3 study. Alzheimers Dement. 2015;11(8):964–74.

[5] Clark CM, Pontecorvo MJ, Beach TG, Bedell BJ, Coleman RE, Doraiswamy PM, et al. Cerebral PET with florbetapir compared with neuropathology at autopsy for detection of neuritic amyloid-β plaques: a prospective cohort study. Lancet Neurol. 2012;11(8): 669–78.

[6] Wolk DA, Grachev ID, Buckley C, Kazi H, Grady MS, Trojanowski JQ, et al. Association between in vivo fluorine 18-labeled flutemetamol amyloid positron emission tomography im-aging and in vivo cerebral cortical histopathology. Arch Neurol. 2011;68(11):1398–403.

[7] European Medicines Agency. Amyvid: florbetapir (18F). Authorisation details. 1999. http://www.ema.europa.eu/ema/index.jsp?curl=pages/medicines/human/medicines/002422/human_med_001611.jsp&mid=WC0b01ac058001d124. Accessed 11 Jun 2017.

[8] European Medicines Agency. Neuraceq: florbetaben (18F). Authorisation details. 1999. http://www.ema.europa.eu/ema/index.jsp?curl=pages/medicines/human/medicines/002553/human_med_001716.jsp&mid=WC0b01ac058001d124. Accessed 11 Jun 2017.

[9] European Medicines Agency. Vizamyl: flutemetamol (18F). Authorisation details. 1999. http://www.ema.europa.eu/ema/index.jsp?curl=pages/medicines/human/medicines/002557/human_med_001794.jsp&mid=WC0b01ac058001d124. Accessed 11 Jun 2017.

[10] Nelissen N, Van Laere K, Thurfjell L, Owenius R, Vandenbulcke M, Koole M, et al. Phase 1 study of the Pittsburgh compound B derivative 18F-flutemetamol in healthy volunteers and patients with probable Alzheimer disease. J Nucl Med. 2009;50(8):1251–9.

[11] Bourgeat P, Villemagne VL, Dore V, Brown B, Macaulay SL, Martins R, et al. Comparison of MR-less PiB SUVR quantification methods. Neurobiol Aging. 2015;36:S159–66.

[12] Camus V, Payoux P, Barré L, Desgranges B, Voisin T, Tauber C, et al. Using PET with 18F-AV-45 (florbetapir) to quantify brain amyloid load in a clinical environment. Eur J Nucl Med Mol Imaging. 2012;39(4):621–31.

[13] Hutton C, Declerck J, Mintun MA, Pontecorvo MJ, Devous MD Sr, Joshi AD; Alzheimer's Disease Neuroimaging Initiative. Quantification of 18F-florbetapir PET: comparison of two analysis methods. Eur J Nucl Med Mol Imaging. 2015;42(5):725–32.

[14] Thurfjell L, Lilja J, Lundqvist R, Buckley C, Smith A, Vandenberghe R, et al. Automated quantification of 18F-flutemetamol PET activity for categorizing scans as negative or positive for brain amyloid: concordance with visual image reads. J Nucl Med. 2014;55(10):1623–8.

[15] Chincarini A, Sensi F, Rei L, Bossert I, Morbelli S, Guerra UP, et al. Standardized uptake value ratio-independent evaluation of brain amyloidosis. J Alzheimers Dis. 2016;54(4):1437–57.

[16] Barthel H, Luthardt J, Becker G, Patt M, Hammerstein E, Hartwig K, et al. Individualized quantification of brain β-amyloid burden: results of a proof of mechanism phase 0 florbetaben PET trial in patients with Alzheimer's disease and healthy controls. Eur J Nucl Med Mol Imaging. 2011;38(9):1702–14.

[17] Saint-Aubert L, Nemmi F, Péran P, Barbeau EJ, Payoux P, Chollet F, et al. Comparison between PET template-based method and MRI-based method for cortical quantification of florbetapir (AV-45) uptake in vivo. Eur J Nucl Med Mol Imaging. 2014;41(5):836–43.

[18] van Berckel BN, Ossenkoppele R, Tolboom N, Yaqub M, Foster-Dingley JC, Windhorst AD, et al. Longitudinal amyloid imaging using 11C-PiB: methodologic considerations. J Nucl Med. 2013;54(9):1570–6.

[19] Becker GA, Ichise M, Barthel H, Luthardt J, Patt M, Seese A, et al. PET quantification of 18F-florbetaben binding to β-amyloid deposits in human brains. J Nucl Med. 2013;54(5):723–31.

[20] Matsubara K, Ibaraki M, Shimada H, Ikoma Y, Suhara T, Kinoshita T, et al. Impact of spillover from white matter by partial volume effect on quantification of amyloid deposition with 11C PiB PET. Neuroimage. 2016;143:316–24.

[21] Rodell AB, O'Keefe G, Rowe CC, Villemagne VL, Gjedde A. Cerebral blood flow and Aβ-amyloid estimates by WARM analysis of 11C PiB uptake distinguish among and between neurodegenerative disorders and aging. Front Aging Neurosci. 2017;8:321.

[22] Tiepolt S, Hesse S, Patt M, Luthardt J, Schroeter ML, Hoffmann KT, et al. Early [(18)F]florbetaben and [(11)C]PiB PET images area surrogate biomarker of neuronal injury in Alzheimer's disease.Eur J Nucl Med Mol Imaging. 2016;43(9):1700–9.

[23] Hsiao IT, Huang CC, Hsieh CJ, Hsu WC, Wey SP, Yen TC, et al. Correlation of early-phase 18F-florbetapir (AV-45/Amyvid) PET images to FDG images: preliminary studies. Eur J Nucl Med Mol Imaging. 2012;39:613–20.

[24] Segonne F, Dale AM, Busa E, Glessner M, Salat D, Hahn HK, et al. A hybrid approach to the skull stripping problem in MRI. Neuroimage. 2004;22:1060–75.

[25] Fischl B, Salat DH, Busa E, Albert M, Dieterich M, Haselgrove C, et al. Whole brain segmentation: automated labeling of neuroanatomical structures in the human brain. Neuron. 2002;33:341–55.

[26] Fischl B, Salat DH, van der Kouwe AJ, Makris N, Ségonne F, Quinn BT, et al. Sequence-independent segmentation of magnetic resonance images. Neuroimage. 2004;23(Suppl 1):S69–84.

[27] Sled JG, Zijdenbos AP, Evans AC. A nonparametric method for automatic correction of intensity nonuniformity in MRI data. IEEE Trans Med Imaging. 1998;17:87–97.

[28] Fischl B, Liu A, Dale AM. Automated manifold surgery: constructing geometrically accurate and topologically correct models of the human cerebral cortex. IEEE Trans Med Imaging. 2001;20:70–80.

[29] Segonne F, Pacheco J, Fischl B. Geometrically accurate topology-correction of cortical surfaces using nonseparating loops. IEEE Trans Med Imaging. 2007;26:518–29.

[30] Desikan RS, Segonne F, Fischl B, Quinn BT, Dickerson BC, Blacker D, et al. An automated labeling system for subdividing the human cerebral cortex on MRI scans into gyral based regions of interest. Neuroimage. 2006;31:968–80.

[31] Fischl B, Dale AM. Measuring the thickness of the human cerebral cortex from magnetic resonance images. Proc Natl AcadSci U S A. 2000;97(20):11050–5.

[32] Mazziotta JC, Toga AW, Evans AC, Fox P, Lancaster J, Zilles K, et al. A four-dimensional probabilistic atlas of the human brain. J Am Med Inform Assoc. 2001;8(5):401–30.

[33] Rullmann M, Dukart J, Hoffmann KT, Luthardt J, Tiepolt S, Patt M, et al. Partial volume effect correction improves quantitative florbetaben beta-amyloid PET scan analysis. J Nucl Med. 2016;57(2):198–203.

[34] Thomas BA, Erlandsson K, Modat M, Thurfjell L, Vandenberghe R, Ourselin S, et al. The importance of appropriate partial volume correction for PET quantification in Alzheimer's disease. Eur J Nucl Med Mol Imaging. 2011;38(6):1104–19.

[35] Rousset OG, Ma Y, Evans AC. Correction for partial volume effects in PET: principle and validation. J Nucl Med. 1998;39(5):904–11.

[36] Rousset OG, Collins DL, Rahmim A, Wong DF. Design and implementation of an automated partial volume correction in PET: application to dopamine receptor quantification in the normal human striatum. J Nucl Med. 2008;49(7):1097–106.

[37] Brendel M, Högenauer M, Delker A, Sauerbeck J, Bartenstein P, Seibyl J, et al. Improved longitudinal [(18)F]-AV45 amyloid PET by white matter reference and VOI-based partial volume effect correction. Neuroimage. 2015;108:450–9.

[38] Teipel S, Drzezga A, Grothe MJ, Barthel H, Chételat G, Schuff N, et al. Multimodal imaging in Alzheimer's disease: validity and usefulness for early detection. Lancet Neurol. 2015;14(10):1037–53.

[39] Joshi AD, Pontecorvo MJ, Lu M, Skovronsky DM, Mintun MA, Devous MD Sr, et al. Semiautomated method for quantification of F18 florbetapir PET images. J Nucl Med. 2015;56(11):1736–41.

[40] Schain M, Varnäs K, Cselényi Z, Halldin C, Farde L, Varrone A. Evaluation of two automated methods for PET region of interest analysis. Neuroinformatics. 2014;12(4):551–62.

[41] Lilja J, Thurfjell L, Sörensen J. Visualization and quantification of 3-dimensional stereotactic surface projections for 18F-Flutemetamol PET using variable depth. J Nucl Med. 2016;57(7): 1078–83.

[42] Lundqvist R, Lilja J, Thomas BA, Lötjönen J, Villemagne VL, Rowe CC, et al. Implementation and validation of an adaptive tem-plate registration method for 18F-flutemetamol imaging data. J Nucl Med. 2013;54(8):1472–8.

[43] Zhou L, Salvado O, Dore V, Bourgeat P, Raniga P, Macaulay SL, et al. MR-less surface-based amyloid assessment based on 11C PiB PET. PLoS One. 2014;9(1):e84777.

[44] Edison P, Carter SF, Rinne JO, Gelosa G, Herholz K, Nordberg A, et al. Comparison of MRI based and PET template based ap-proaches in the quantitative analysis of amyloid imaging with PIB-PET. Neuroimage. 2013;70:423–33.

[45] Akamatsu G, Ikari Y, Ohnishi A, Nishida H, Aita K, Sasaki M, et al. Automated PET-only quantification of amyloid deposition with adaptive template and empirically pre-defined ROI. Phys Med Biol. 2016;61(15):5768–80.

[46] Su Y, D'Angelo GM, Vlassenko AG, Zhou G, Snyder AZ, Marcus DS, et al. Quantitative analysis of PiB-PET with FreeSurfer ROIs. PLoS One. 2013;8(11):e73377.

[47] Tuszynski T, Rullmann M, Luthardt J, Butzke D, Tiepolt S, Gertz HJ, et al. Evaluation of software tools for automated identification of neuroanatomical structures in quantitative β-amyloid PET imag-ing to diagnose Alzheimer's disease. Eur J Nucl Med Mol Imaging. 2016;43(6):1077–87.

[48] Su Y, Blazey TM, Snyder AZ, Raichle ME, Hornbeck RC, Aldea P, et al. Quantitative amyloid imaging using image-derived arterial input function. PLoS One. 2015;10(4):e0122920.

[49] Ikoma Y, Edison P, Ramlackhansingh A, Brooks DJ, Turkheimer FE. Reference region automatic extraction in dynamic [(11)C]PIB. J Cereb Blood Flow Metab. 2013;33(11):1725–31.

[50] Heurling K, Buckley C, Van Laere K, Vandenberghe R, Lubberink M. Parametric imaging and quantitative analysis of the PET amy-loid ligand [(18)F]flutemetamol. Neuroimage. 2015;121:184–92.

[51] Su Y, Blazey TM, Owen CJ, Christensen JJ, Friedrichsen K, Joseph-Mathurin N, et al. Quantitative amyloid imaging in autoso-mal dominant Alzheimer's disease: results from the DIAN study group. PLoS One. 2016;11(3):e0152082.

[52] Arnold SE, Hyman BT, Flory J, Damasio AR, Van Hoesen GW. The topographical and neuroanatomical distribution of neurofibril-lary tangles and neuritic plaques in the cerebral cortex of patients with Alzheimer's disease. Cereb Cortex. 1991;1:103–16.

[53] Braak H, Braak E. Neuropathological stageing of Alzheimer-related changes. ActaNeuropathol. 1991;82:239–59.

[54] Serrano-Pozo A, Frosch MP, Masliah E, Hyman BT. Neuropathological alterations in Alzheimer disease. Cold Spring HarbPerspect Med. 2011;1(1):a006189.

[55] Chételat G, Ossenkoppele R, Villemagne VL, Perrotin A, Landeau B, Mézenge F, et al. Atrophy, hypometabolism and clinical trajec-tories in patients with amyloid-negative Alzheimer's disease. Brain. 2016;139(Pt 9):2528–39.

[56] Rowe CC, Ellis KA, Rimajova M, Bourgeat P, Pike KE, Jones G, et al. Amyloid imaging results from the Australian imaging, bio-markers and lifestyle (AIBL) study of aging. Neurobiol Aging. 2010;31(8):1275–83. doi:10.1016/j.neurobiolaging.2010.04.007.

[57] Cecchin, D., Barthel, H., Poggiali, D., Cagnin, A., Tiepolt, S., Zucchetta, P., Turco, P., Gallo, P., Frigo, A.C., Sabri, O. and Bui, F., 2017. A new integrated dual time-point amyloid PET/MRI data analysis method. European journal of nuclear medicine and molecular imaging, 44(12), pp.2060-2072.